The effect of the lattice spacing change on cross-bridge kinetics in chemically skinned rabbit psoas muscle fibers

II. Elementary steps affected by the spacing change

Yan Zhao and Masataka Kawai
Department of Anatomy, The University of Iowa, College of Medicine, Iowa City, Iowa 52242 USA

ABSTRACT The actin-myosin lattice spacing of rabbit psoas fibers was osmotically compressed with a dextran T-500, and its effect on the elementary steps of the cross-bridge cycle was investigated. Experiments were performed at the saturating Ca (pCa 4.5–4.9), 200 mM ionic strength, pH 7.0, and at 20°C, and the results were analyzed by the following cross-bridge scheme:

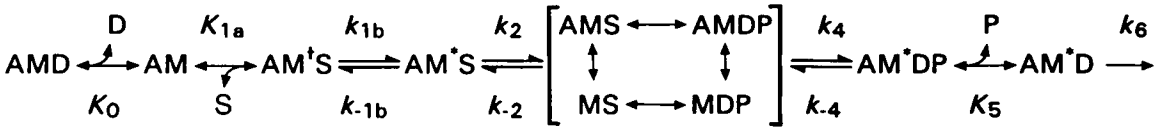

where A = actin, M = myosin head, S = MgATP, D = MgADP, and P = Pi = phosphate. From MgATP and MgADP studies on exponential process (C) and (D), the association constants of cross-bridges to MgADP (K_0), MgATP (K_{1a}), the rate constants of the isomerization of the AM†S state (k_{1b} and k_{-1b}), and the rate constants of the cross-bridge detachment step (k_2 and k_{-2}) were deduced. From Pi study on process (B), the rate constants of the cross-bridge attachment (power stroke) step (k_4 and k_{-4}) and the association constant of Pi ions to cross-bridges (K_5) were deduced. From ATP hydrolysis measurement, the rate constant of ADP-isomerization (rate-limiting) step (k_6) was deduced. These kinetic constants were studied as functions of dextran concentrations. Our results show that nucleotide binding, the ATP-isomerization, and the cross-bridge detachment steps are minimally affected by the compression. The rate constant of the reverse power stroke step (k_{-4}) decreases with mild compression (0–6.3% dextran), presumably because of the stabilization of the attached cross-bridges in the AM*DP state. The rate constant of the power stroke step (k_4) does not change with mild compression, but it decreases with higher compression (>6.3% dextran), presumably because of an increased difficulty in performing the power stroke. These results are consistent with the observation that isometric tension increases with a low level of compression and decreases with a high level of compression. Our results also show that the association constant K_5 of Pi with cross-bridge state AM*D is not changed with compression. Our result further show that the ATP hydrolysis rate decreased with compression, and that the rate constants of the ADP-isomerization step (k_6) becomes progressively less with compression. The effect of compression on the power stroke step and rate-limiting step implies that a large-scale molecular rearrangement in the myosin head takes place in these two slow reaction steps.

INTRODUCTION

In our previous work with sinusoidal analysis in skinned muscle fibers, we established a cross-bridge scheme that is consistent with the effects of MgATP, MgADP, and inorganic phosphate (Pi) on exponential processes (B), (C), and (D) (Kawai and Halvorson, 1989, 1991; Kawai and Zhao 1992). These are summarized in scheme 1 (following), which consists of seven cross-bridge states with seven elementary steps that represent transitions between the states.

Scheme 1

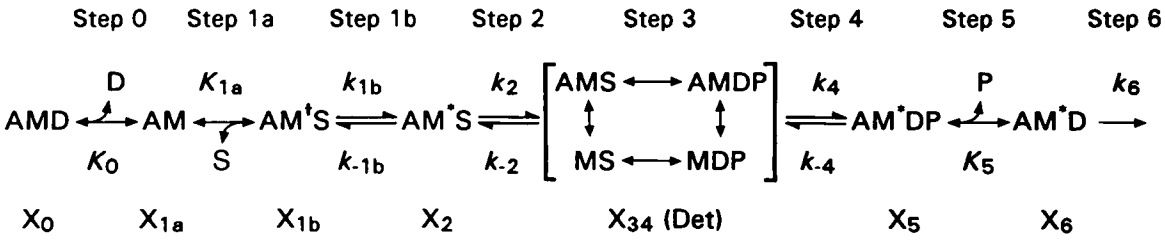

where A = actin, M = myosin head, S = MgATP, D = MgADP, and P = Pi = phosphate. An asterisk (*) or a dagger (†) identifies the second (and the third) conformational state(s). X_i is the steady state probability of cross-bridges in the respective states. In step 1a, the substrate (S) binds to the cross-bridge state AM to form a collosion complex AM†S, and in step 1b, AM†S isomerizes to form the AM*S state (ATP isomerization step). Cross-bridges detach at step 2 to form the Det (X_{34}) state. Det includes all detached states (MS, MDP) and "weakly attached" states (AMS, AMDP) (Greene and

Address correspondence to Dr. Masataka Kawai, Department of Anatomy, The University of Iowa, College of Medicine, Iowa City, IA 52242, USA.

Eisenberg, 1980; Schoenberg, 1988). We found that the apparent rate constant $2\pi d$ reflects the transition between AM†S and AM*S states, the apparent rate constant $2\pi c$ reflects the transition between AM*S and Det states, and both are sensitive to MgATP and MgADP concentrations. In step 4, cross-bridge attach to form AM*DP state, and this is followed by Pi-release (step 5) to form AM*D state. We found that the apparent rate constant $2\pi b$ reflects the transition between Det and AM*DP states (attachment step 4), and is sensitive to Pi and MgATP concentrations; this step corresponds to the power stroke step (Kawai and Halvorson, 1991). We further found that the binding of nucleotides (MgATP, MgADP) and Pi is faster than our speed of observation, hence steps 0, 1a, and 5 can be approximated by equilibria. Step 6 is the ADP-isometrization step, and it is the slowest step of the cross-bridge cycle. Scheme 1 uniquely explains our data, and there is no other scheme that can explain the data with the same degree of simplicity. With sinusoidal analysis, we were able to determine three association constants and six rate constants of steps 0–5; with the ATP hydrolysis rate measurement, we were able to determine the rate constants of step 6.

Several years ago, we reported that low compression increased isometric tension and high compression decreased the tension in rabbit psoas fibers (Kawai and Schulman, 1985). Because the apparent rate constants decreased with compression, we hypothesized that low levels of compression decreased the cross-bridge detachment rate and high levels of compression decreased the cross-bridge attachment rate. When this work was published, we were not able to demonstrate whether a decrease in the detachment rate was related directly to the cross-bridge detachment step or to the reversal of the cross-bridge attachment step. Likewise, we were not able to demonstrate whether a decrease in the attachment rate was related directly to the cross-bridge attachment step or to the reversal of the cross-bridge detachment step. As we described above, we recently succeeded in constructing a cross-bridge scheme in skinned fibers and deducing the kinetic constants. Therefore, we are in a position to test our earlier hypotheses and to identify the specific elementary step(s) that are altered by the lattice spacing change, and to examine whether the particular effect on the elementary step is consistent with the change in isometric tension. Preliminary accounts of the present study have been presented (Zhao and Kawai 1991; Zhao et al. 1993).

MATERIALS AND METHODS

Chemicals and solutions

The sources of chemicals are the same as those used for the fiber width study in our companion paper (Paper I, Methods). In addition, we purchased P^1, P^5-di(adenosine-5′)pentaphosphate (A_2P_5), L-lactic dehydrogenase (LDH), phospho(enol) pyruvate (KPEP), pyruvate kinase (PK), and NaN_3 from Sigma Chemical Co. (St Louis, MO). The reduced form of alpha-nicotineamide adenine dinucleotide (NADH) was purchased from Boehringer Mannheim Biochemicals (Indianapolis, IN). The relaxing solution, the control activation solution, and the rigor solutions are the same as in paper I. The wash solution contained (mM): 0.5 MgATP, 8 KPi, 102 KProp, 75 NaProp, and 10 MOPS. The solution composition of each individual experiment is found in the Results section. The dextran concentration is expressed as a percent (%), which indicates grams of dextran added to 100 ml of solution (g/dl). Individual concentrations of multivalent ionic species were calculated using our computer program, which assumed multiple equilibria with the following apparent association constants (log values at pH 7.00): CaEGTA 6.28, MgEGTA 1.61, CaATP 3.70, MgATP 4.00, CaADP 2.65, MgADP 2.84, CaCP 1.15, MgCP 1.30, CaPEP 1.99, and MgPEP 2.17. Metal binding constants for PEP were calculated based on values given by Vianna (1975). pCa of activating solutions was in the range of 4.5–4.9.

Fiber preparations

The method of preparing rabbit psoas bundles and their skinning procedure were described in paper I. Preparations consisting of one or two fibers were dissected from a bundle and used for experiments. For the MgATP and Pi studies, fibers were mounted by wrapping them around two clamps made of stainless steel wire (360 μm in diameter) in the relaxing solution (Kawai and Brandt, 1980). For the MgADP studies and ATP hydrolysis rate measurements, the ends of the fibers were double-knotted, and each end was placed in a hook made of tungsten wire (125 μm in diameter) with a gap of about 100 μm. There were no differences in the complex modulus data when these two methods were tested with the control activating solution, indicating that the end effects were not contributing factors to our complex modulus data. The sarcomere length of the fibers was adjusted to 2.5 μm by optical diffraction using an He–Ne laser (Spectra-Physics, Mountainview, CA), and then the length of the preparations (L_0) was measured. For the MgATP and Pi studies, the fiber cross-sectional area was estimated by assuming an elliptical shape. The major and minor diameters of the ellipse of each fiber were measured by an ocular micrometer at a magnification of 200, using Nomarsky optics on a Leitz Diavert compound microscope (Ernst Leitz Wetzlar GmbH, Wetzlar, Germany). The major diameter was measured at the middle of the fibers, and the minor diameter was measured at the wrapped ends. For the MgADP studies, the diameter seen from the top was used, and the circular cross-section was assumed. The purpose of the diameter measurement was to give the best estimate for the cross-sectional area to calculate tension of the control activation (T_c). Since all the data were normalized to T_c, and the kinetics are not affected by the cross-sectional area, conclusions in our papers will not change even if there were some errors in the estimate of the cross-sectional area.

Sinusoidal analysis

The preparation in the relaxing solution was washed with washing solution, then replaced with the activating solution that contained dextran T-500 but no CaEGTA. The baseline record of the complex modulus was collected at this time, and the width of the fiber at a fixed point along the fiber was measured. Then the full volume of solution was replaced with the activating solution that contained 6 mM CaEGTA and 0.9 times the dextran concentration. The dextran concentration was reduced in this solution, because concentrated CaEGTA (66 mM) was added to the dextran solution 1:10 by volume. When a steady tension developed, an experimental record of the complex modulus was collected, and the width of the fiber at the same fixed point was measured again. Then the fiber was relaxed with the relaxing solution without dextran. The complex modulus $Y(f)$ was defined as the ratio of the stress change to the strain change expressed in the frequency domain. $Y(f)$ was fitted to an equation consisting of four exponential processes:

$$Y(f) = H + \underbrace{A/(1 + a/fi) - B/(1 + b/fi)}_{\text{Process (A)}} \quad \underbrace{\qquad}_{\text{Process (B)}}$$

$$\underbrace{+ C/(1 + c/fi) + D/(1 + d/fi)}_{\text{Process (C)}} \quad \underbrace{\qquad}_{\text{Process (D)}} \quad (1)$$

$$Y_\infty = H + A - B + C + D \quad (2)$$

where f is the frequency of sinusoidal length oscillation. Peak-to-peak amplitude was fixed to 0.25% L_0 in our reports. We denote characteristic frequencies of respective processes by a, b, c, d, and their magnitudes by A, B, C, D. $i = \sqrt{-1}$, and 2π times characteristic frequencies represent apparent (observed) rate constants. Because we expanded the frequency range (0.25–350 Hz), an additional exponential process (D) was necessary to describe the complex modulus data (Abbot and Steiger, 1977; Ford et al., 1977; Shimizu and Tanaka, 1984). The results of the data fitting is compared in Fig. 1 with (Fig. 1 *C*) and without (Fig. 1 *B*) process (D). It is apparent from this figure that the complex modulus data in the mid and high frequency ranges is described more precisely when process (D) is included in the fitting equation. Y_∞ is the complex modulus extrapolated to the infinite frequency, and it does not have an imaginary part. This quantity is referred to as "stiffness" in our reports, and it is proportional to the number of attached cross-bridges. Y_∞ corresponds to phase 1, process (D) to the fast components of phase 2, process (C) to the slow component of phase 2, process (B) to phase 3, and process (A) to phase 4 of step analysis (Huxley and Simmons 1971; Heinl et al. 1974). The detail of the sinusoidal analysis method were published previously (Kawai and Brandt, 1980). At both the beginning and the end of each series of experiments, the preparation was tested with the control activating solution to examine the reproducibility of the data. Tension was detected by a deflection of a gauge element (AE 801; Aker Micro Electronics, Horten, Norway), and the resonance frequency of the tension transducer assembly was 1.5 KHz (Kawai and Brandt, 1980), which correlates to 9400 s^{-1} in the rate constant domain. All experiments were performed at 20°C.

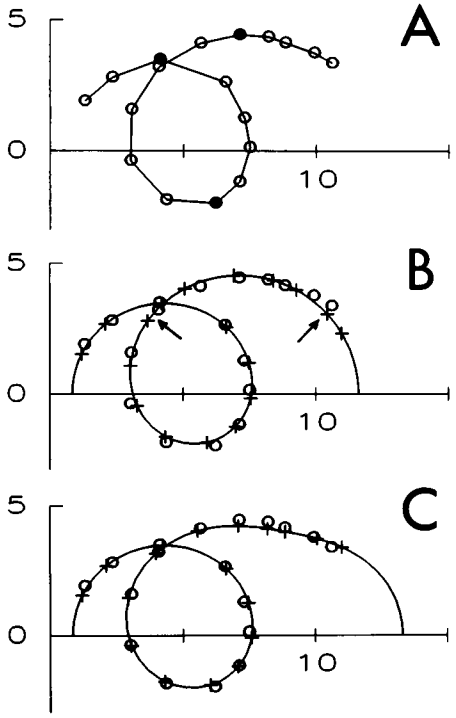

FIGURE 1 Complex modulus data of activated preparation by the control activating solution in the absence of dextran are displayed in the Nyquist plot. Abscissi represent the elastic modulus (units: MN/m^2) and ordinate represents the viscous modulus (units: MN/m^2). Circles (O) represent observed data averaged over 11 experiments, and pluses (+) and smooth curves represent theoretical projections. Areas of mismatch between the observed data and the theoretical values are indicated by arrows. The complex modulus data were corrected against rigor. (*A*) Experimental results. Lines are drawn to connect individual frequency points, and decade frequencies (1, 11, and 100 Hz) are shown in filled circles. (*B*) Data are fitted to Eq. 1 without process (*D*). (*C*) Data are fitted to Eq. 1 with 4 exponential processes. Frequency points used are, in the clockwise direction, 0.25, 0.5, 1, 2, 3.1, 5, 7.1, 11, 17, 25, 35, 50, 70, 100, 135, 187, 250, and 350 Hz.

ATP hydrolysis rate measurements

The apparatus and the signal processing procedure to measure the ATP hydrolysis rate is modified from Güth and Wojciechowski (1986). ATP hydrolysis is coupled with NADH oxidation in the presence of PEP, PK, and LDH (Takashi and Putnam, 1979). In this reaction mixture, one mole each of PEP and NADH are consumed as one mole of ATP is hydrolyzed and rephosphorylated, and one mole each of lactate, phosphate, and NAD are produced. A decrease in the NADH concentration is followed by its fluorescence. The absolute ATP hydrolysis rate of the fibers (mM/sec) was calculated according to the equation:

$$\text{ATP hydrolysis rate} = C\frac{fA}{Fa}$$

where C is the concentration of NADH (1.2 mM), F is the fluorescence signal from NADH at this concentration (adjusted to 5–8 V with a solution that contained in mM: 1.2 NADH, 6 EGTA, 2 MgATP, 5 free ATP, 8 KPi, 62 NaProp, 48 KProp, 10 MOPS, pH 7.00; this solution did not contain PEP, PK, or LDH), f is the decline of the fluorescence signal (V/s), A is the cross-sectional area of the cuvette (1 mm^2), and a is the cross-sectional area of the fibers. The tension cost is defined as the ratio of the ATP hydrolysis rate to the isometric tension. Experiments were performed at 20°C.

RESULTS

Effect of compression on isometric tension and stiffness

The correlation between the Dextran T-500 concentration and the fiber width/lattice spacing was already shown in paper I. The effects of compression on isometric tension and stiffness (Y_∞) in control activating solution are shown in Fig. 2. At lower levels of compression, isometric tension increased and peaked at 6.3% dextran (Fig. 2 *A*). The peak tension corresponded to 1.23 *Tc*, where *Tc* is the tension of the control activation in the absence of dextran (*Tc* averaged to 207 ± 8 kN/m^2; N = 112, ±SEM). Compression with 3–5% T-500 achieves the lattice spacing of intact muscle fibers (Matsubara et al., 1985; see Discussion). With further compression, the isometric tension decreased, becoming 0.49 *Tc* at 14.4% dextran. The stiffness Y_∞ calculated by Eq. 2 increased with compression and peaked at 11.7% dextran (Fig. 2 *B*). The peak stiffness amounted to 157% compared to that without compression. At the highest level of compression (14.4% dextran) stiffness somewhat decreased, but this decrease was not significant. These re-

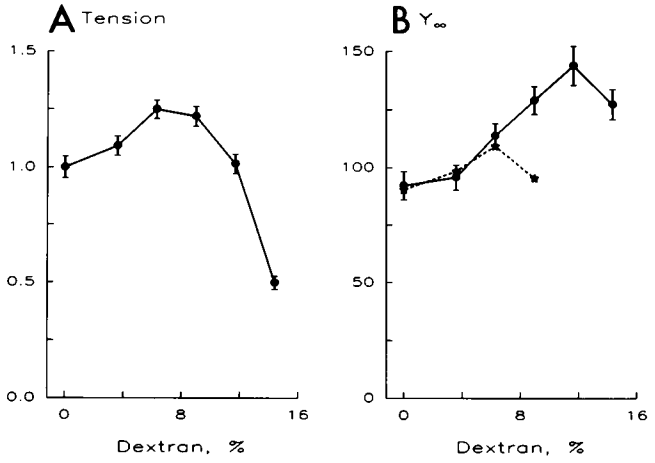

FIGURE 2 Isometric tension (A) and stiffness Y_∞ (B) versus dextran T-500 concentration (*circles* and *solid lines*). The average of 11 experiments is shown with SEM error bars. Broken lines and stars in B represent the population of attached cross-bridges (see the Discussion). Units of the ordinates are T_c.

sults are generally consistent with those of earlier reports (Krasner and Maughan, 1984; Gulati and Babu, 1985; Kawai and Schulman, 1985).

Effect of MgATP on rate constant $2\pi c$ and $2\pi d$ at different levels of compression

To characterize the kinetic constants involved in the MgATP binding step 1a, isomerization step 1b, and the cross-bridge detachment step 2, the MgATP concentration was changed at fixed dextran concentrations, and the rate constants $2\pi c$ and $2\pi d$ were obtained. The effect of MgATP was studied in the concentration range from 0.1 to 10 mM. Individual solutions were created by appropriately mixing two extreme solutions 0S and 10S, where S denotes the millimolar concentration of $MgATP^{2-}$ ions. 0S solution contained (mM): 5.0 free ATP, 40 KProp, and 38 NaProp. 10S solution contained (mM): 10.6 MgATP, 4.4 free ATP, 30 KProp, and 18 NaProp. In addition, both solutions contained (mM): 6 CaEGTA (pCa 4.82–4.84), 8 KPi, 15 CP, 10 MOPS, and 160 units/ml of CK. Our computer calculation demonstrates that there is no significant ionic rearrangements with this mixing. The high Pi concentration (8 mM) was chosen, because, more cross-bridges are distributed in the states AM, AM†S, AM*S, and Det (scheme 1), hence the resolution of processes (C) and (D) is improved. The resulting complex modulus data were analyzed by Eq. 1, and the rate constants $2\pi c$ and $2\pi d$ were obtained. These are plotted in Fig. 3 (solid points and SEM error bars) against MgATP concentration at four levels of compression. These plots reveal that their MgATP dependence is hyperbolic: both $2\pi c$ and $2\pi d$ increased at low millimolar concentrations, and they approached saturation by 5–10 mM. Such MgATP dependence can be explained by steps 1a through 2 in scheme 1. From scheme 1, the apparent rate constants are deduced as follows (see Eqs. 29 and 35 in Appendix):

$$2\pi d = \frac{K_{1a}S}{1 + K_0D + K_{1a}S}k_{1b} + k_{-1b} \quad (3)$$

$$2\pi c = \frac{K_{1b}K_{1a}S}{1 + K_0D + (1 + K_{1b})K_{1a}S}k_2 + k_{-2} \quad (4)$$

where S represents the MgATP concentration, k_{1b} represents the forward rate constant of the ATP-isomerization step 1b, k_{-1b} represents the backward rate constant of the isomerization, and $K_{1b} = k_{1b}/k_{-1b}$. k_2 represents the forward rate constant of the cross-bridge detachment step 2, k_{-2} represents the backward rate constant of the detachment, and $K_2 = k_2/k_{-2}$. The data in Fig. 3 were fitted to Eqs. 3 and 4 by assuming $D = 0$, and the kinetic constants were deduced. The continuous lines in Fig. 3 represent theoretical projections based on the best fit parameters and Eqs. 3 and 4. The best fit parameters were obtained by fitting all available data points. The kinetics constants were then normalized to that in the absence of dextran, and plotted in Fig. 4 as functions of dextran T-500 concentrations. This figure demonstrates that the association constant K_{1a} and the rate constants k_{1b}, k_{-1b}, k_2, and k_{-2} are minimally affected by compression. The kinetic constants in the absence of dextran are summarized in Table 1.

Effect of MgADP on rate constants $2\pi c$ and $2\pi d$ at different levels of compression

To characterize the association constant involved in the MgADP binding (step 0), the MgADP concentration was changed (0–8 mM) at fixed MgATP (5 mM) and dextran concentrations, and the rate constants of $2\pi c$ and $2\pi d$ were obtained. Individual solutions were created by appropriately mixing two extreme solutions 0D and 8D, where D denotes the millimolar concentration of MgADP. 0D solution contained (mM): 0.3 $MgProp_2$, 66 NaProp, and 69 KProp. 8D solution contained (mM): 8 ADP, 3.5 $MgProp_2$, 54 NaProp, and 47 KProp. In addition, both solutions contained (mM): 6 CaEGTA (pCa 4.54–4.64), 6.1 MgATP, 0.2 A_2P_5, 8 KPi, and 10 MOPS. Mg^{2+} ion concentration was maintained at 1 mM to ensure that most ATP and ADP molecules chelated Mg^{2+}. A_2P_5(0.2 mM) was added to inhibit adenylate kinase activity (Lienhard and Secemski, 1973; Feldhaus et al., 1975). The MgADP study was repeated in four different dextran concentrations (0, 3.6, 6.3, and 9%). In Fig. 5 the rate constants $2\pi c$ and $2\pi d$ are plotted against the MgADP concentration at four different levels of compression. The results were fitted to Eqs. 3 and 4 to deduce K_0 utilizing K_{1a} obtained from the MgATP study at corresponding dextran concentrations.

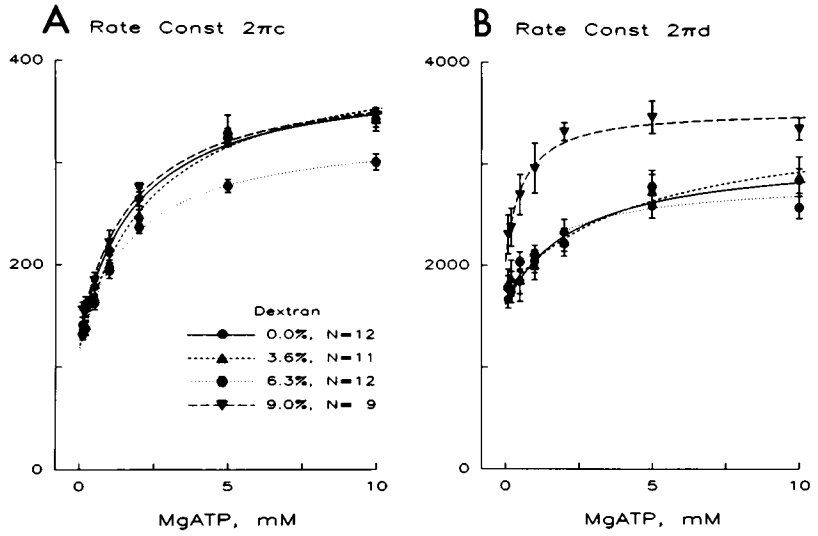

FIGURE 3 The apparent rate constants $2\pi c$ (A) and $2\pi d$ (B) are plotted against MgATP concentration at four different dextran concentrations as indicated in A. Symbols indicate averaged values, and error bars indicate SEM. The curves are based on Eq. 4 (A) or Eq. 3 (B) and the best fit parameters. Units of the ordinates are s^{-1}.

The association constant K_0 was normalized to that in the absence of dextran and entered in Fig. 4 A. The value of K_0 in the absence of dextran is listed in Table 1. It is apparent in Fig. 4 A that the effect of compression on K_0 is small for the dextran concentration in the range of 0–6.3%, but the effect appears to be larger (2.2 times) at the 9% dextran concentration.

As reported by Kawai and Halvorson (1989), the longevity of fibers was poor in solutions that contained ADP, and the control isometric tension reproduced only within 60–70% after the MgADP study. In contrast, the longevity of fibers was excellent in solutions that contained CP and CK, and the control isometric tension reproduced within 80–100% after the MgATP study.

Effect of phosphate (Pi) on rate constant $2\pi b$ at different levels of compression

In our previous report, we demonstrated that the exponential process (B) represents the cross-bridge attachment step 4 and Pi release step 5 (Kawai and Halvorson,

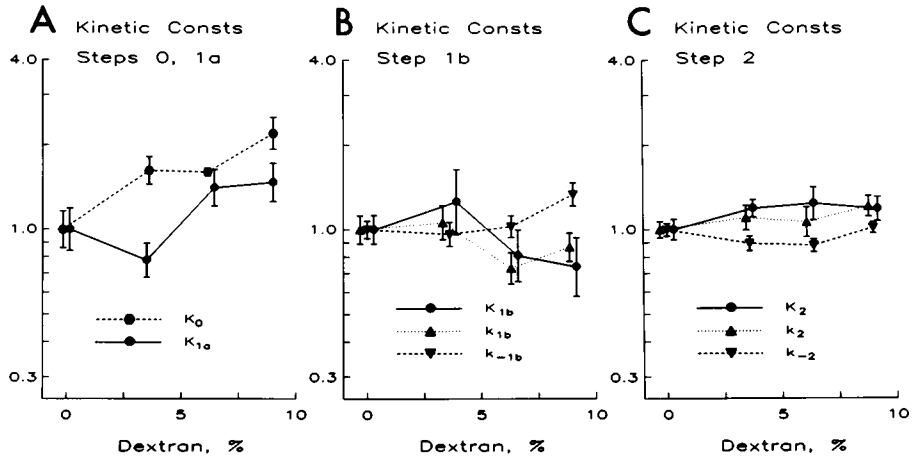

FIGURE 4 The effect of compression on the kinetic constants of steps 0–2. Data were averaged and normalized to that at the 0% dextran concentration and plotted with SEM error bars in a logarithmic scale. (A) The association constants K_0 for MgADP (based on the MgADP study on $2\pi c$, N = 7–9) and K_{1a} for MgATP (based on the MgATP study on $2\pi c$, N = 9–12) are plotted against the dextran concentration. (B) The rate constants (k_{1b}, k_{-1b}) and the equilibrium constant (K_{1b}) of ATP-isomerization step 1b are plotted against the dextran concentration. The data were based on the MgATP study on $2\pi d$ (N = 9–11). (C) The rate constants (k_2, k_{-2}) and the equilibrium constant (K_2) of the cross-bridge detachment step 2 are plotted against the dextran concentration. The data were based on the MgATP study on $2\pi c$ (N = 9–12).

TABLE 1 **Kinetic constants that specify scheme 1**

Constant	Source	Best fit	Average ± SEM (*N*)	Units
K_0	ATP/c	0.530	0.58 ± 0.09 (7)	mM^{-1}
K_{1a}	ATP/c	0.262	0.23 ± 0.04 (10)	mM^{-1}
k_{1b}	ATP/d	1530	1880 ± 220 (10)	s^{-1}
k_{-1b}	ATP/d	1610	1510 ± 110 (10)	s^{-1}
K_{1b}	ATP/d	0.95	1.29 ± 0.15 (10)	
k_2	ATP/c	536	510 ± 30 (10)	s^{-1}
k_{-2}	ATP/c	130	132 ± 7 (10)	s^{-1}
K_2	ATP/c	4.12	3.9 ± 0.3 (10)	
k_4	Pi/b	105.7	106 ± 4 (11)	s^{-1}
k_{-4}	Pi/b	87.6	90 ± 5 (11)	s^{-1}
K_4	Pi/b	1.207	1.20 ± 0.07 (11)	
K_5	Pi/b	0.181	0.19 ± 0.02 (11)	mM^{-1}
k_6	ATPase	16.2	16.2 ± 1.3 (18)	s^{-1}

The kinetic constants in the absence of dextran are listed. The best fit parameters were obtained after fitting all the available data to respective equations and used for the calculation of the theoretical curves. The averaged parameters were obtained by fitting the individual experiment to respective equations. The results were then averaged.

1991), and process (B) is sensitive to the Pi concentration. In the same report, we showed that this attachment generates force, hence it is also called the "power stroke step." In order to characterize the role of the lattice spacing change in these elementary steps, we studied the effect of Pi on the exponential process (B) at four different dextran T-500 concentrations (0, 3.6, 6.3, and 9%). For this Pi study, two extreme Pi solutions (0P and 16P) were created initially, and then intermediate solutions were created as an appropriate mixture of these two solutions. 0P solution contained 53 mM KProp, and 16P solution contained (mM): 16 Pi and 16 KProp; and both solutions contained (mM): 6 CaEGTA (pCa 4.82), 5.3 MgATP, 4.7 free ATP, 28 NaProp, 15 CP, 10 MOPS, and 160 units/ml CK. The high MgATP concentration (5 mM) was chosen, because more cross-bridges are distributed in the states Det, AM*DP and AM*D (Scheme 1), hence the resolution of process (B) is improved.

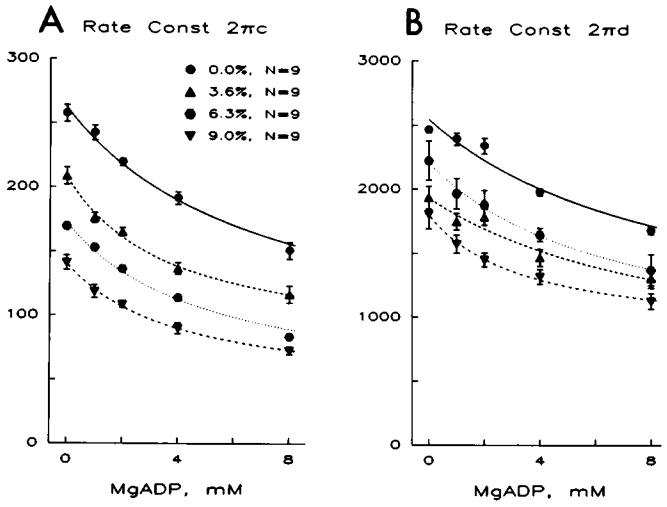

FIGURE 5 The apparent rate constants $2\pi c$ (*A*) and $2\pi d$ (*B*) are plotted against the MgADP concentration at four different dextran concentrations as indicated in *A*. Symbols indicate averaged values, and error bars indicate SEM. The curves are based on Eq. 4 (*A*) or Eq. 3 (*B*) and the best fit parameters. Units of the ordinates are s^{-1}.

When the apparent rate constant $2\pi b$ is plotted against Pi concentration (Fig. 6), the plot is curved (concave downward). This relationship is explained by Eq. 5, which is based on scheme 1. The derivation of Eq. 5 is shown in the Appendix (Eq. 41).

$$2\pi b = \sigma k_4 + \epsilon k_{-4} \tag{5}$$

where

$$\sigma = \frac{K_{1b}K_2K_{1a}S}{1 + K_0D + (1 + K_{1b} + K_{1b}K_2)K_{1a}S} \tag{6}$$

and

$$\epsilon = \frac{K_5P}{1 + K_5P}. \tag{7}$$

As seen here, the Pi dependence of $2\pi b$ is manifested via ϵ (Eq. 7), and the MgATP dependence via σ (Eq. 6). When Eq. 5 is plotted against the Pi concentration (Fig. 6 *A*), the intercept to the ordinate (Pi = 0) represents the rate constant of the power stroke step (k_4) multiplied by the constant factor σ. This factor is in the vicinity of 1 for the Pi study that utilizes a large concentration of

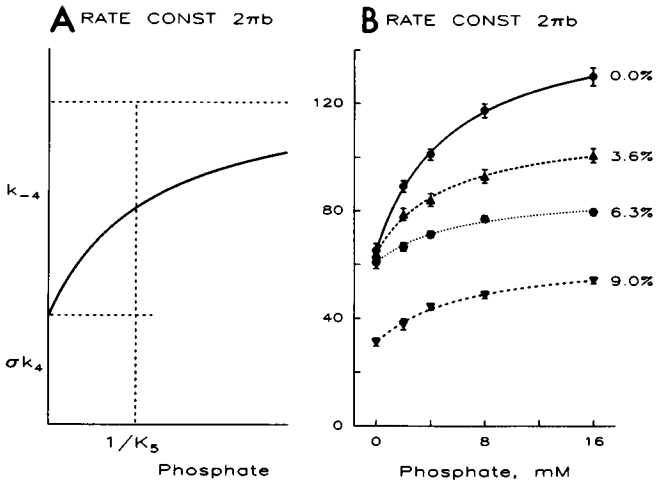

FIGURE 6 (*A*) The theoretical projection of Eq. 5. The apparent rate constant $2\pi b$ is plotted against the Pi concentration. This figure demonstrates the method of interpreting the data in Fig. 6 *B*. σ is defined in Eq. 6, and σ = 0.614 in the absence of dextran. (*B*) Experimental results. The apparent rate constant $2\pi b$ is plotted against Pi concentration at four different dextran concentrations as indicated. Symbols indicate the averaged values, and error bars indicate SEM. Error bars smaller than the symbol size cannot be seen. The number of observations are 11 (0.0% dextran condition), 10 (3.6%), 8 (6.3%), and 9 (9.0%). The curves are based on Eq. 5 and the best fit parameters. The units of the ordinate: s^{-1}.

MgATP, similar to the one used in the current report (5 mM), and if $K_2 > 1$. The increment to the large Pi concentration (ϵ: 0 → 1) represents the rate constant of the reverse power stroke step (k_{-4}). The Pi concentration at half-saturation point ($\epsilon = 0.5$) is the dissociation constant of Pi from the cross-bridge state AM*DP (step 5), and its reciprocal is the association constant K_5. The averaged $2\pi b$ as a function of Pi at different dextran concentrations is shown in Fig. 6 *B* with discrete symbols and error bars (±SEM). The results were fitted to Eq. 5 to deduce k_4, k_{-4}, and K_5. For the calculation of σ, the equilibrium constants (K_{1a}, K_{1b}, and K_2) obtained from MgATP studies at the corresponding dextran concentrations were used, and $S = 5$ mM, D = 0 mM were assumed. The theoretical values based on the best fit parameters are entered as smooth curves in Fig. 6 *B;* the best fit parameters were obtained by fitting all available data points to Eq. 5. The kinetic constants without compression are summarized in Table 1, and their relative changes with compression are shown in Fig. 7.

As seen in Fig. 7 *A*, the rate constant of the power stroke step (k_4) does not change significantly at low levels of compression with 0–6.3% dextran, and it declines markedly at a high level of compression with 9% dextran. In contrast, the rate constant of the reversal step (k_{-4}) decreases significantly at low levels of compression, followed by a slight (but insignificant) increase at high levels of compression. These changes in the rate constants result in a threefold increase in the equilibrium constant ($K_4 = k_4/k_{-4}$) of step 4 at low levels of compression, followed by a decrease in the equilibrium constant at high levels of compression. Because step 4 leads into force generation (Kawai and Halvorson, 1991), this change in K_4 is consistent with the change in isometric tension shown in Fig. 2 *A*. The association constant of Pi to cross-bridges (K_5) does not change with compression (Fig. 7 *B*).

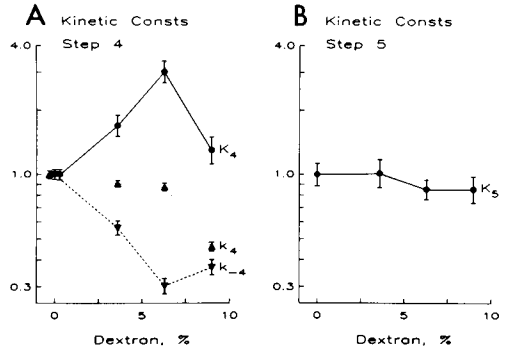

FIGURE 7 The effect of compression on the kinetic constants of steps 4 and 5. Data were averaged and normalized to that at the 0% dextran condition, and plotted with SEM error bars in a logarithmic scale. The data were based on Pi study on $2\pi b$ ($N = 8$–11). (*A*) The rate constants (k_4, k_{-4}) and the equilibrium constant (K_4) of the cross-bridge attachment step 4 are plotted against dextran concentration. (*B*) The association constant K_5 for Pi is plotted against dextran concentration.

TABLE 2 **Effect of dextran T-10 on the apparent rate constants**

App Rate Const	0%	0.45%
$2\pi a$	5.58 ± 0.39	5.26 ± 0.25
$2\pi b$	140 ± 2	137 ± 2
$2\pi c$	309 ± 9	302 ± 8
$2\pi d$	2570 ± 190	2420 ± 140

Units: s^{-1} ± SEM is shown for $N = 7$.

The effect of lower MW fraction of dextran on cross-bridge kinetics

According to the manufacture's specification, a dextran fraction is not homogeneous and its molecular weight (mol wt) is distributed. Because the lower mol wt fraction of dextran T-500 could enter the lattice space, it might be suspected that this fraction increases the viscosity of the solution surrounding the myosin head, which in turn might create an effect on the cross-bridge kinetics (Endo et al., 1979). Our paper I concluded that the upper limit of mol wt that enters the lattice space is about 20 kD, based on the dextran T-10 and T-40 experiments. According to the manufacturer's mol wt distribution chart, the lowest mol wt of dextran T-500 plotted is 60 kD, and the fraction ≤ 60 kD is present at the 2% level. From this, we estimate that the fraction with mol wt less than 20 kD is present at <0.7% level in T-500. The corresponding upper limit in 9% T-500 solution is 0.06% (0.7% of 9%). To examine if the effect of compression on cross-bridge kinetice at 9% T-500 was based on the lower mol wt fraction that entered the actin–myosin lattice space, dextran T-10 was added to the control activating solution (Berman and Maughan, 1982), and the cross-bridge kinetics were studied. We tested a higher concentration of T-10 (0.45%), because we know that about 81% of T-10 enters fiber (paper I), and to account for a possible error in the mol wt distribution chart supplied by the manufacturer. The results are summarized in Table 2. As seen in this table, the effect of 0.45% T-10 is very little, and the apparent rate constants are not any different from those in the absence of dextran. Certainly, the effect on $2\pi b$ (Table 2) is far less than that of T-500 (Fig. 6 *B*). From this experiment, we conclude that the major effect we saw on T-500 was not based on the lower mol wt fraction that entered the lattice space.

Distribution of cross-bridges among various cross-bridge states

Based on Eqs. 16–22 (Appendix), we calculated the steady-state distribution (probability) of cross-bridges among various states at four levels of compression (Fig. 8). The equilibrium constants used are the averaged values shown in Table 1 in the absence of dextran and those shown in Figs. 4 and 7 in the presence of dextran. The probability for the AMD state (X_0) is not shown, because

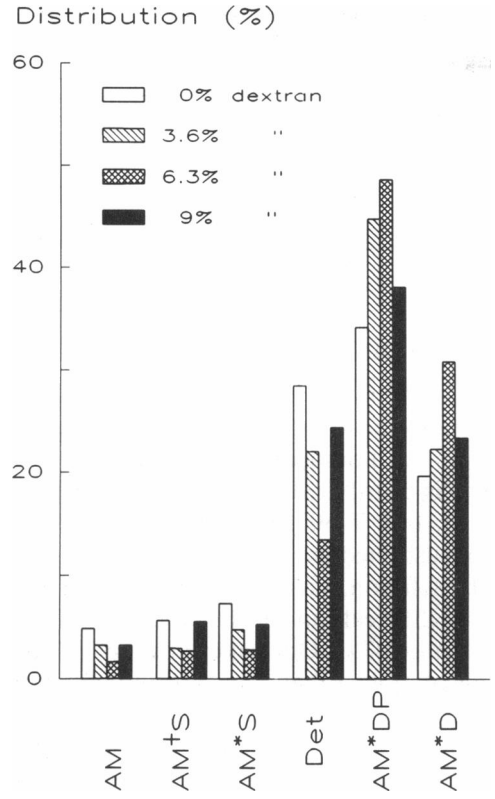

FIGURE 8 Distribution (probability) of cross-bridges among six states at four levels of compression is based on Eqs. 17–23 at 5 mM MgATP, 0 mM MgADP, and 8 mM Pi. Cross-bridge numbers in the AMD state are small (<0.1%) and not shown.

it is less than 0.1% when the MgADP concentration is less than 20 μM (see Eq. 16). In these calculations, we assumed that S = 5 mM, D = 0 mM, and Pi = 8 mM (our control activating condition).

Fig. 8 demonstrates that the probability of cross-bridges in states AM, AM$^+$S, and AM*S is small, and it ranges from 2 to 7%. In contrast, 28% of cross-bridges are detached in the absence of dextran, and this value decreases to 13% in the presence of 6.3% dextran. The cross-bridges are distributed primarily in the AM*DP (34–49%) and AM*D (20–31%) states. These are the major tension (generating) states, and both increase with compression, peak at 6.3% dextran, and decrease again for further compression.

The ATP hydrolysis rate at different levels of compression

We recently showed that step 6 (isomerization of AM*D state; scheme 1) limits the ATP hydrolysis rate in the near isometric condition in skinned rabbit psoas muscle fibers (Kawai and Halvorson, 1991). To determine whether this rate-limiting step is affected by the change in the lattice spacing, we measured the ATP hydrolysis rate at different dextran concentrations. Both relaxing and activating solutions contained (mM): 15 Na_2KPEP, 8 KPi, 10 NaN_3, 28 NaProp, 10 MOPS (pH adjusted to 7.00), 1.2 NADH, 0.18 A_2P_5, 92 U/ml PK, and 130 U/ml LDH. In addition, the activating solution contained (mM): 6 CaEGTA (pCa 4.58), 6.07 MgATP, 1.39 $MgProp_2$, and 33 KProp; the relaxing solution contained (mM): 0.108 CaEGTA, 5.89 EGTA (pCa 8.00), 6.01 MgATP, 1.68 $MgProp_2$, and 32 KProp. The averaged hydrolysis rate is shown in Fig. 9 *A*, isometric tension in Fig. 9 *B*, and the tension cost in Fig. 9 *C*. The ATP hydrolysis rate decreased progressively with an increase in the dextran concentration in the entire range. The isometric tension had a broad peak between 3.6% and 6.3% dextran concentrations, then it declined for a further increase in the dextran concentrations (Fig. 9 *B*). The decrease in the hydrolysis rate was more than that of isometric tension, and resulted in a lower tension cost in the mid and high range of dextran concentration (Fig. 9 *C*).

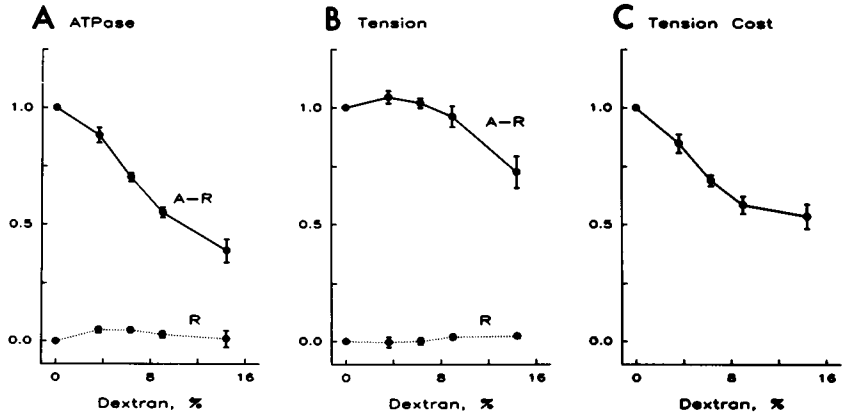

FIGURE 9 The effect of compression on the ATP hydrolysis rate (*A*), the isometric tension (*B*), and the tension cost (*C*). N = 10. The data were normalized to the standard condition (no dextran), then the averaging was performed and shown with the SEM error bars (those smaller than symbol size are not seen). The data collected during relaxation are labeled R. These are subtracted from the data during activation and labeled A-R.

The absolute hydrolysis rate during activation in the absence of dextran averaged 0.64 ± 0.05 mMs^{-1} (N = 18, ±SEM). The isometric tension averaged 141 ± 9 kN/m^2, and the tension cost averaged 4.5 ± 0.2 $\mu mole/J/s$. The corresponding turnover number is 3.2 ± 0.3 s^{-1} per myosin head, if the myosin head (S-1) concentration is assumed to be 0.2 mM (Tregear and Squire, 1973). These values of hydrolysis rate are comparable to our earlier measurements (Kawai et al., 1987, 1990), and they are at the high end of the range reported by other workers on fast-twitch skeletal muscles (Curtin et al., 1974; Arata et al., 1977; Levy et al., 1976; Takashi and Putnam, 1979; Glyn and Sleep, 1985).

The rate constant k_6 was calculated based on the ATP hydrolysis rate of Fig. 9 *A*, and plotted against the dextran concentration in Fig. 10 *A*. We assumed the ATP hydrolysis rate to be $J = [AM^*D]k_6$, and k_6 is plotted in solid lines and circles. The probability of a cross-bridge state AM*D was calculated by Eqs. 22 and 23 in the appendix. In our analysis the reversal reaction of step 6 is ignored, because K_6 is 50–100 in experiment using S-1 (Sleep and Hutton, 1980), and because the cross-bridge in AMD and AM states are small (Fig. 8). Fig. 10 *B* plots the same data as the solid line in Fig. 10 *A* in the log scale, to compare the lattice spacing dependence on k_6 with other kinetic constants in Figs. 4 and 7. The actual number of k_6 in the absence of dextran was 16.3 s^{-1} (Table 1). The rate constant k_6 in Fig. 10 *A* is similar to the tension cost (Fig. 9 *C*). This is because AM*DP and AM*D are major tension generating states, their dependence of compression is similar (Fig. 8), and the cross-bridge distribution in states AM, AM†S, and AM*S are small (Fig. 8) under our activating conditions. In other words, tension cost could represent the rate constants of the rate-limiting step when sufficient MgATP is present in the activating solution.

Fig. 9 *A* and *B* also plots the hydrolysis rate and tension during relaxation (labeled R). As seen in this figure, the hydrolysis rate (<5%) and tension (<2%) during relaxation were much lower than during activation.

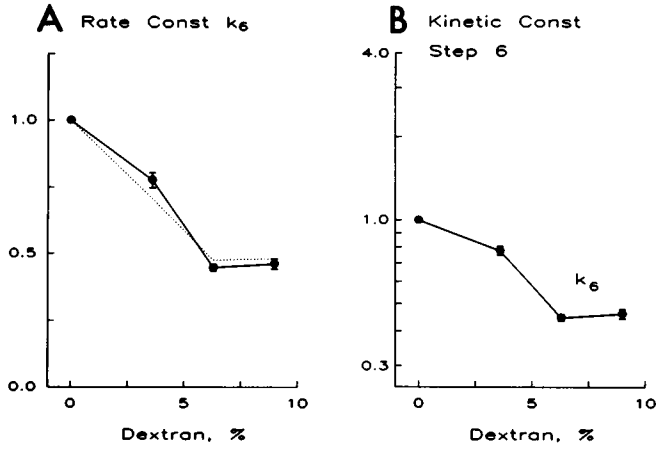

FIGURE 10 The rate constant k_6 is calculated based on the ATP hydrolysis rate of Fig. 9 *A*, and plotted against the dextran concentration. The rate constants are first normalized to that at the control condition (0% dextran), averaged for 10 experiments, and plotted with SEM error bars. In *A*, k_6 is plotted in the linear scale. In *B*, the same result is shown in the log scale.

DISCUSSION

Effect of compression on the elementary steps

The most important observation in the present study is that the rate constant $2\pi b$ of process (B) is affected by the change in actin–myosin lattice spacing (Fig. 6 *B*). This process represents cross-bridge attachment step 4 (power stroke step) and the subsequent Pi-release step 5. With the deduction of the kinetic constants of elementary steps, we were able to specify the elementary step that is affected by the lattice spacing change. Our results show that with low levels of compression (0–6.3% dextran) the rate of the reverse power stroke (k_{-4}) decreases, and with high levels of compression (6.3–9% dextran) the rate of the power stroke (k_4) decreases (Fig. 7 *A*). This causes K_4 ($=k_4/k_{-4}$) to increase at low levels of compression, and to decrease at high levels of compression. As the experiments on T-10 demonstrate (Table 2), the major effect of dextran on the rate constants is based on the lattice spacing change, and the effects are not based on the lower molecular weight fraction of dextran that entered the lattice space.

Since K_4 is directly related to force generation, an increase in force is predicted at low levels of compression, whereas a decrease in force is predicted at high levels of compression. These predictions are in accord with our observation of the isometric tension change with compression (Fig. 2 *A*). From the Pi effect, we deduced the association constant K_5 of Pi to cross-bridges in the AM*D state. Our results (Fig. 7 *B*) show that K_5 is unchanged in the entire dextran concentration range we tested. We infer from this observation that the Pi binding site on the myosin head is not altered by the compression of the lattice spacing.

From the result of MgATP study, we conclude that the lattice spacing change does not affect the MgATP binding step 1a, isomerization step 1b, and subsequent cross-bridge detachment step 2 (Fig. 4). Thus, we conclude that MgATP binding site is not altered by compression, and steps 1a through 2 occur irrespective of the spacing available between the thick and thin filament. The MgADP binding step 0 is slightly increased at low levels of compression, and it appears to increase at high levels of compression with 9% dextran (Fig. 4 *A*). These conclusions are consistent with our earlier observation that the effect of compression was less on process (C) than on process (B) (Kawai and Schulman, 1985).

Effect of compression on Y_∞ (stiffness)

Based on the kinetic constants, we calculated the steady-state distribution (probability) of the cross-bridges in various states (Fig. 8) at four levels of compression. Under our control activating conditions (no dextran), cross-bridges distribute mostly among Det (28%), AM*DP (34%), and AM*D (20%) states. As expected, the number of cross-bridges in the attached states increases with compression, peaks at 6.3% dextran, and decreases again for further compression. Since Y_∞ is the modulus extrapolated to the infinite frequency (Eq. 2), it should register all attached cross-bridges. In other words, Y_∞ should scale with the probability of the sum of all attached cross-bridges:

$$Y_\infty = Y_a(X_0 + X_{1a} + X_{1b} + X_2 + X_5 + X_6) = Y_a(1 - X_{34}) \quad (8)$$

where Y_a is the stiffness of the fiber when all cross-bridges are attached. The calculated stiffness with Eq. 8 is represented in Fig. 2 *B* by a broken line for $Y_a = 126T_c$. As seen in this figure, the data and the prediction agree well up to 6.3% dextran. At higher concentrations the predicted value and observed data diverge. It is apparent from this comparison that the large stiffness values in the highly compressed state are not caused by the usual cross-bridge interaction with actin. Furthermore, the maximum observed stiffness is somewhere between 127 and 144 T_c (Fig. 2 *B*), and not very much higher than $126T_c$ (stiffness when 100% cross-bridges are attached), implying that the extra stiffness is mostly caused by the cross-bridges. We infer from these observations that, when the lattice spacing is highly compressed, the myosin head is squeezed between two sets of filaments, resulting in a large stiffness value but without effecting the normal contact with actin to transduce energy.

The actin–myosin lattice spacing available for cross-bridges

We calculated the available spacing between thick and thin filaments based on equatorial x-ray diffraction studies (paper I) and compared it with the approximate size of the myosin head in Fig. 11. We assumed the diameter of the thin filament to be 9.5 nm (Egelman et al., 1983) and the thick filament to be 15 nm. Since the center-to-center distance between the two sets of filaments is 26.4 nm (paper I, Fig. 3) during rigor and without dextran, the spacing from surface-to-surface is 14.2 nm [26.4 − (15 + 9.5)/2]. Note that the width during Ca activation and after rigor induction is just about the same in the absence of dextran (paper I, Fig. 5). This spacing value seems to be small compared to the known size of the myosin head that is tadpole-shaped with the long axis measuring 16.5 nm (Winkelmann et al., 1991). The actual spacing available for the myosin head to interact with actin must be somewhat larger than 14.2 nm (probably by 3–4 nm), because the side of the head rather than the tip interacts with actin. Thus, it is likely that the neck region of the S-1 head is not on the thick filament, and that there is an extra degree of freedom at the neck where S-1 connects to S-2. This situation is depicted in Fig. 11 *A*. In this case, the myosin head may attach to actin to generate force; however, the head may come off easily because of the thermal vibration. This will result in a large k_{-4}. It is known that the cross-bridge force is generated in the diagonal direction (Schoenberg, 1980), and the force can be divided into longitudinal and radial elements. We can then visualize that the radial element helps the fiber shrink on Ca activation as observed at low dextran concentrations (paper I, Fig. 5 *B*). Our finding, that the forward rate constant (k_4) does not change significantly at low levels of compression, is consistent with the observation that the neck region of the myosin head is flexible; when there is adequate spacing between the head and the thin filaments, the distance change seems not to hinder the attachment rate (step 4) of the head to the thin filament as long as the thin filament is within reach.

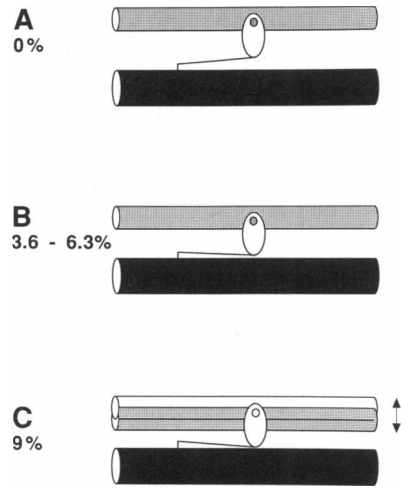

FIGURE 11 The relationship between the myosin head (S-1), S-2, and the thick and thin filaments. Percent (%) indicates the dextran concentration. This drawing is based on the actual dimension of each component.

At low levels of compression (3.6%–6.3% dextran), the neck region of the myosin head may be pressed against the thick filament (Fig. 11 *B*), hence the thermal motion of the myosin head becomes limited and results in a smaller k_{-4} (Fig. 6 *A*). Since force is generated at step 4, a smaller k_{-4} will result in a larger force, as we have observed (Fig. 2 *A*). With equatorial x-ray diffraction studies, Matsubara et al. (1985) reported that d_{10} spacing in intact murine toe muscle is 37.5 nm in Tyrode solution at sarcomere length 2.5 μm. The center-to-center distance of thick and thin filaments is then 25.0 nm. This spacing corresponds to that in 4.3% dextran

solution, based on Fig. 3 of paper I. Thus, we conclude that the condition depicted in Fig. 11 *B* is close to the living muscles, and that the distance is optimal for the force generation.

The spacing between thick and thin filaments becomes very small (Fig. 11 *C*) when the fibers are highly compressed by dextran (9% or more). Under these conditions, it may be difficult for the myosin head to make the correct contact with actin to perform the power stroke reaction (step 4). This will result in a lower k_4 as we have observed (Fig. 7 *A*). The critical power stroke reaction may occur only when adequate spacing becomes available. This is possible because the thin filaments are flexible in the radial direction, and they exhibit thermal fluctuations (Fujime and Ishiwata, 1971; Oosawa et al., 1973). The degree of fluctuation even increases when Ca is bound to the thin filaments (Ishiwata and Fujime, 1972). If the power stroke reaction occurs, then the lattice spacing is fixed at this larger value, which will result in an apparent expansion of the fiber width as observed (Fig. 5 *B*, paper I). Because of the difficulty of this power stroke reaction, the active force in highly compressed fiber is lower than that without compression, as reported previously (Godt and Maughan, 1981; Krasner and Maughan, 1984; Kawai and Schulman, 1985) and in this paper (Fig. 2 *A*, Fig. 9 *B*).

Rate-limiting step

Our earlier analysis concluded that the step exiting from the AM*D state is the slowest reaction among forward reactions in the cross-bridge cycle (Kawai and Halvorson, 1991). This conclusion was based on our observation that the MgATP, MgADP, and Pi effects on exponential processes (B), (C), and (D) are all consistent with scheme 1, provided that step 6 is the slowest reaction of all forward reactions in the cross-bridge cycle. If we assume step 6 is faster, then the MgATP, MgADP, and Pi effects could not be explained. Thus step 6 is the rate-limiting step. In our analysis, the rate-limiting step is either the isomerization of the AM*D state, which results in the formation of the AMD state, or the MgADP desorption step directly from the AM*D state, which results in the formation of the AM state. The presence of two energetically different AMD states was recognized in the isolated and reconstituted acto-S1 system (Sleep and Hutton, 1980). For simplicity, we developed the discussion in this paper equating the rate-limiting step to the ADP-isomerization step, but the discussion is equally valid if the ADP-isomerization is replaced by ADP-desorption.

The rate-limiting step is characterized by the ATP hydrolysis rate measurement. Our results show that the hydrolysis rate during Ca activation is significantly reduced as the lattice spacing is compressed by dextran (Fig. 9 *A*). Our results are similar to observations by other investigators on different muscle types. Krasner and Maughan (1984) studied Ca^{2+}-activated force and ATP hydrolysis rate in skinned rabbit soleus muscle fibers when they were compressed by dextran T-500. Similarly, Arheden et al. (1987) studied these parameters in taenia coli muscle of the guinea pig. We conclude from these observations that the interaction between the lattice spacing and the kinetics surrounding the rate limiting step are similar whether the muscle type is fast twitch skeletal, slow twitch skeletal, or smooth. However, the ATP hydrolysis rate during relaxation was significantly lower in psoas than in taenia coli, demonstrating that the relaxation is far more complete in skeletal than in smooth muscles.

There are two possible mechanisms that the ATP hydrolysis rate can be affected by compression. One is that the rate constant k_6 is reduced by compression. The other is that the probability of cross-bridges in AM*D is reduced by compression. Our analysis in Fig. 8 demonstrates that the AM*D decreases with compression. Our further analysis in Fig. 10 demonstrates that k_6 also decreases with compression. Thus, it can be concluded that both of these mechanisms underlie the reduced hydrolysis rate with compression. The decrease in the AM*D state is possible because of a decrease in K_4 as discussed above. The decrease in k_6 is possible if the ADP-isomerization step requires a large-scale rearrangement such as in the shape of the myosin head. If this is the case, the spacing between thick and thin filament becomes a critical factor in the rearrangement process. This possibility is strengthened when we recognize that the myosin head spends the most time in the AM*D state, because step 6 is the slowest step of all forward reactions in the cross-bridge cycle. Consequently, there is an adequate time for filament sliding and muscle shortening to occur while the cross-bridges are at the AM*D state. Evidently, such motion would require a large-scale molecular rearrangement, hence it is reasonable to be sensitive to the available spacing between the thick and thin filaments.

It may be suspected that process (A) observed in our sinusoidal analysis and phase 4 in the step analysis (Huxley and Simmons, 1971; Heinl et al., 1974) might represent the rate-limiting step. The apparent rate constant $2\pi a$ is 5.58 sec^{-1} at 20°C (Table 2), and it is not remote from our measured k_6 (16 sec^{-1}). However, there are difficulties in this hypothesis, because a coherent model to equate process (A) to step 6 cannot be built based on the same principles as employed in the present studies, and because process (A) disappears on a partial (−20%) cross-linking of the myosin heads to the thin filaments while the muscle's ability to perform oscillatory work is enhanced (Tawada and Kawai, 1990). Thus, it is not likely that process (A) (phase 4) corresponds to the rate-limiting step. Process (A) probably represents large-scale sarcomere rearrangements, including filament sliding (Tawada and Kawai, 1990).

CONCLUSION

We conclude that the cross-bridge attachment step 4 and ADP-isomerization step 6 are modified by compression, whereas the ligand (MgATP, MgADP, Pi) binding steps 0, 1a, 5, and other faster reactions (steps 1b and 2) are not sensitive to compression. Thus, it can be generalized that two slowest reaction steps in the cross-bridge cycle are sensitive to available spacing for myosin cross-bridges. These two steps are important in the cycle, because force is generated at step 4, and work is performed at step 6. From the facts that these steps interfere with the available spacing between the thick and thin filaments, we infer that both steps require large-scale rearrangements in the conformation of the contractile proteins, most likely in the shape of the myosin head. From the fact that these steps are slow, we infer that the large-scale rearrangement may take time to progress. The slow reaction speed is also convenient to perform work on the external world, which needs seconds rather than milliseconds to overcome the inertia. The slow speed would be further convenient to perform a delicate control of the motion, using the feedback network involving the central nervous system.

APPENDIX

Steady-state solution of scheme 1

The steady-state solution can be obtained by assuming the mass action law (equilibrium) as an approximation for steps 0–5 and by assuming $k_6 = 0$. The mass action law cannot be applied to the rate-limiting step 6:

$$X_{1a} = X_0/K_0D \tag{9}$$

$$X_{1b} = X_{1a}K_{1a}S \tag{10}$$

$$X_2 = X_{1b}K_{1b} \tag{11}$$

$$X_{34} = X_2K_2 \tag{12}$$

$$X_5 = X_{34}K_4 \tag{13}$$

$$X_6 = X_5/K_5P. \tag{14}$$

In addition, since X_i are probabilities (conservation rule).

$$X_0 + X_{1a} + X_{1b} + X_2 + X_{34} + X_5 + X_6 = 1. \tag{15}$$

From Eqs. 9–15, we obtain:

$$X_0 = K_0DK_5P/M \tag{16}$$

$$X_{1a} = K_5P/M \tag{17}$$

$$X_{1b} = K_{1a}SK_5P/M \tag{18}$$

$$X_2 = K_{1a}SK_{1b}K_5P/M \tag{19}$$

$$X_{34} = K_{1a}SK_{1b}K_2K_5P/M \tag{20}$$

$$X_5 = K_{1a}SK_{1b}K_2K_4K_5P/M \tag{21}$$

$$X_6 = K_{1a}SK_{1b}K_2K_4/M \tag{22}$$

where

$$M = K_{1a}SK_{1b}K_2K_4 + K_5P[1 + K_0D + K_{1a}S(1 + K_{1b} + K_{1b}K_2 + K_{1b}K_2K_4)]. \tag{23}$$

If we do not assume the mass action law for step 0–5, then the steady-state solution can be obtained in a more complex way ($k_6 \neq 0$). Results of such analysis indicate that the fractional error on the probability of a cross-bridge state based on the above method is less than J/k_s under our experimental condition, where J is the ATP hydrolysis rate (3.2 s^{-1}), and k_s is the slowest reaction of step 0–5. This is k_{-4} (87.6 s^{-1}) in Table 1. Thus, the upper limit of the error is 0.037 X_i. This level of error does not change significantly the cross-bridge distribution shown in Fig. 8, and it does not have a major impact on any of the conclusions developed in this paper.

Transient solution of step 1b

For the time (t) dependent transient solution for each cross-bridge state, we use the lower case letter $x_i(t)$ to denote the deviation from the steady-state probability X_i. When we focus on the frequencies that characterize step 1b (process D), steps 0 and 1a are faster, hence these steps can be approximated by the mass action law, and Eqs. 9 and 10 can be directly applied to x_i. Evidently, Eq. 11 is not applicable. Steps 2, 4, and 6 are much slower than step 1b, hence they effectively do not occur for frequencies that characterize process (D). This procedure isolates steps 2–6 from step 1b. Thus, the master equation that characterizes step 1b is:

$$\dot{x}_0 + \dot{x}_{1a} + \dot{x}_{1b} = -k_{1b}x_{1b} + k_{-1b}x_2 = -\dot{x}_2 \tag{24}$$

where a dot ($\cdot$) above x_i indicates differentiation with respect to the time ($\dot{x} = dx/dt$). The conservation rule is:

$$x_0 + x_{1a} + x_{1b} + x_2 = 0. \tag{25}$$

After substituting Eqs. 9 and 10 into Eq. 24, we obtain:

$$\dot{x}_{1b}/\beta = -k_{1b}x_{1b} + k_{-1b}x_2 = -\dot{x}_2 \tag{26}$$

where

$$\beta = \frac{K_{1a}S}{1 + K_0D + K_{1a}S}.$$

If we similarly substitute Eqs. 9 and 10 into Eq. 25, we obtain:

$$x_{1b}/\beta + x_2 = 0. \tag{27}$$

If we eliminate x_2 from Eqs. 26 and 27, we obtain:

$$\dot{x}_{1b} = -(\beta k_{1b} + k_{1b})x_{1b} \tag{28}$$

After solving Eq. 28, we obtain:

$$x_{1b} = D_1 \exp(-2\pi dt)$$

where D_1 is the integration constant. The apparent rate constant is

$$2\pi d = \beta k_{1b} + k_{-1b} \tag{29}$$

Eq. 29 is the same as Eq. 3

Transient solution of step 2

When we focus on the frequencies that characterize step 2 (process C), steps 0–1b are faster. Thus these steps can be approximated by the mass action law, and Eqs. 9–11 can be directly applied to x_i. Evidently, Eq.

12 is not applicable. Steps 4 and 6 are slower than step 2, so we assume that they effectively do not occur for frequencies that characterize process (C). This procedure isolates steps 4–6 from step 2. Thus, the master equation that characterizes step 2 is:

$$\dot{x}_0 + \dot{x}_{1a} + \dot{x}_{1b} + \dot{x}_2 = -k_2x_2 + k_{-2}x_{34} = -\dot{x}_{34} \quad (30)$$

and the conservation rule is:

$$x_0 + x_{1a} + x_{1b} + x_2 + x_{34} = 0. \quad (31)$$

After substituting Eqs. 9–11 into Eq. 30, we obtain:

$$\dot{x}_2/\alpha = -k_2x_2 + k_{-2}x_{34} = -\dot{x}_{34} \quad (32)$$

where

$$\alpha = \frac{K_{1a}SK_{1b}}{1 + K_0D + (1 + K_{1b})K_{1a}S}.$$

If we similarly substitute Eqs. 9–11 into Eq. 31, we obtain:

$$x_2/\alpha + x_{34} = 0. \quad (33)$$

If we eliminate x_{34} from Eqs. 32 and 33, we obtain:

$$\dot{x}_2 = -(\alpha k_2 + k_{-2})x_2. \quad (34)$$

After solving Eq. 34, we obtain

$$x_2 = C_1 \exp(-2\pi ct)$$

where C_1 is the integration constant. The apparent rate constant is

$$2\pi c = \alpha k_2 + k_{-2}. \quad (35)$$

Eq. 35 is the same as Eq. 4.

Transient solution of step 4

When we focus on the frequencies that characterize step 4 (process B), steps 0–2 are faster, hence these steps can be characterized by the mass action law, and Eqs. 9–12 can be directly applied to x_i; the same holds true for step 5 (Eq. 14). Evidently, Eq. 13 is not applicable. Step 6 is much slower than step 4, and it effectively does not occur for frequencies that characterize process (B). Therefore, the master equation that characterizes step 4 is:

$$\dot{x}_0 + \dot{x}_{1a} + \dot{x}_{1b} + \dot{x}_2 + \dot{x}_{34} = -k_4x_{34} + k_{-4}x_5 = -\dot{x}_5 - \dot{x}_6. \quad (36)$$

After substituting Eqs. 9–12 and 14 into Eq. 36, we obtain:

$$\dot{x}_{34}/\sigma = -k_4x_{34} + k_{-4}x_5 = -\dot{x}_5/\epsilon \quad (37)$$

where σ and ϵ are defined in Eqs. 6 and 7. The conservation rule is:

$$x_0 + x_{1a} + x_{1b} + x_2 + x_{34} + x_5 + x_6 = 0. \quad (38)$$

If we similarly substitute Eqs. 9–12 and 14 into Eq. 38, we obtain:

$$x_{34}/\sigma + x_5/\epsilon = 0. \quad (39)$$

If we eliminate x_5 from Eqs. 37 and 39, we obtain:

$$\dot{x}_{34} = -(\sigma k_4 + \epsilon k_{-4})x_{34}. \quad (40)$$

After solving Eq. 40, we obtain:

$$x_{34} = B_1 \exp(-2\pi bt)$$

where B_1 is the integration constant. The apparent rate constant is

$$2\pi b = \sigma k_4 + \epsilon k_{-4}. \quad (41)$$

Eq. 41 is the same as Eq. 5. Eqs. 29, 35 and 41 can be obtained directly from scheme 1 by the method described by Hammes (1968).

The present work was supported by grant AR21530 from the National Institutes of Health and grant DCB90-18096 from the National Science Foundation.

Received for publication 11 November 1991 and in final form 18 September 1992.

REFERENCES

Abbott, R. H., and G. J. Steiger. 1977. Temperature and amplitude dependence of tension transients in glycerinated skeletal and insect fibrillar muscle. *J. Physiol.* 266:13–42.

Arata, T., Y. Mukohata, and Y. Tonomura. 1977. Structure and function of the two heads of the myosin molecule. VI. ATP hydrolysis, shortening, and tension development of myofibrils. *J. Biochem. (Tokyo).* 82:801–812.

Arheden, H., A. Arner, and P. Hellstrand. 1987. Force-velocity relation and rate of ATP hydrolysis in osmotically compressed skinned smooth muscle of the guinea pig. *J. Muscle Res. Cell Motil.* 8:151–160.

Berman, M. R., and D. W. Maughan. 1982. Axial elastic modulus as a function of relative fiber width in relaxed skinned skeletal muscle fibers. *Pfluegers Arch.* 393:99–103.

Curtin, N. A., C. Gilbert, K. M. Kretzschmar, and D. R. Wilkie. 1974. The effect of the performance of work on total energy output and metabolism during muscular contraction. *J. Physiol. (Lond.).* 238:455–472.

Egelman, E. H., N. Francis, and D. J. DeRosier. 1983. Helical disorder and the filament structure of F-actin are elucidated by the angle-layered aggregate. *J. Mol. Biol.* 116:605–629.

Endo, M., T. Kitazawa, and Y. Kakuta. 1979. Effect of "viscosity" of the medium on mechanical properties of skinned skeletal muscle fibers. *In* Cross-Bridge Mechanisms in Muscle Contraction. H. Sugi and G. H. Pollack, editors. University of Tokyo Press, Tokyo. 365–374.

Feldhaus, P., T. Fröhlich, R. S. Goody, M. Isakov, and R. H. Schirmer. 1975. Synthetic inhibitors of adenyl kinases in the assays for ATP-ases and phosphokinases. *Eur. J. Biochem.* 57:197–204.

Ford, L. E., A. F. Huxley, and R. M. Simmons. 1977. Tension responses to sudden length change in stimulated frog muscle fibres near slack length. *J. Physiol.* 269:441–515.

Fujime, S., and S. Ishiwata. 1971. Dynamic study of F-actin by quasielastic scattering of laser light. *J. Mol. Biol.* 62:251–265.

Glyn, H., and J. Sleep. 1985. Dependence of adenosine triphosphatase activity of rabbit psoas muscle fibres and myofibrils on substrate concentration. *J. Physiol. (Lond.).* 365:259–276.

Godt, R. E., and Maughan, D. W. 1981. Influence of osmotic compression on calcium activation and tension in skinned muscle fibers of the rabbit. *Pfluegers Arch. Eur. J. Physiol.* 391:334–337.

Greene, L. E., and E. Eisenberg. 1980. Cooperative binding of myosin subfragment-1 to the actin-troponin-tropomyosin complex. *Proc. Natl. Acad. Sci. USA.* 77:2616–2620.

Gulati, J., and A. Babu. 1985. Critical dependence of calcium-activated force on width in highly compressed skinned fibers of the frog. *Biophys. J.* 48:781–787.

Güth, K., and R. Wojciechowski. 1986. Perfusion cuvette for the simultaneous measurement of mechanical, optical and energetic parameters of skinned muscle fibers. *Pfluegers Arch.* 407:552–557.

Hammes, G. G. 1968. Relaxation spectrometry of biological systems. *Adv. Prot. Chem.* 23:1–57.

Heinl, P., H. J. Kuhn, and J. C. Rüegg. 1974. Tension responses to quick length changes of glycerinated skeletal muscle fibres from the frog and tortoise. *J. Physiol. (Lond.).* 237:243–258.

Huxley, A. F., and R. M. Simmons. 1971. Proposed mechanism of force generation in striated muscle. *Nature (Lond.).* 233:533–538.

Ishiwata, S., and S. Fujime. 1972. Effect of calcium ions on the flexibility of reconstituted thin filaments of muscle studied by quasielastic scattering of laser light. *J. Mol. Biol.* 68:511–522.

Kawai, M. and P. W. Brandt. 1980. Sinusoidal analysis: a high resolution method for correlating biochemical reactions with physiological processes in activated skeletal muscles of rabbit, frog and crayfish. *J. Muscle Res. Cell Motil.* 1:279–303.

Kawai, M. and R. Halvorson. 1989. Role of MgATP and MgADP in the cross-bridge kinetics in chemically skinned rabbit psoas fibers. Study of a fast exponential process (C). *Biophys. J.* 55:595–603.

Kawai, M., and H. R. Halvorson. 1991. Two step mechanism of phosphate release and the mechanism of force generation in chemically skinned fibers of rabbit psoas muscle. *Biophys. J.* 59:329–342.

Kawai, M. and M. I. Schulman. 1985. Cross-bridge kinetics in chemically skinned rabbit psoas fibers when the actin-myosin lattice spacing is altered by dextran T-500. *J. Muscle Res. Cell Motil.* 6:313–332.

Kawai, M., and Y. Zhao. 1992. Tension per cross-bridge state deduced from sinusoidal analysis. *Biophys. J.* 61:A292 (Abstr).

Kawai, M., K. Güth, K. Winnikes, C. Haist and J. C. Rüegg. 1987. The effect of inorganic phosphate on the ATP hydrolysis rate and the tension transients in chemically skinned rabbit psoas fibers. *Pfluegers Archiv.* 408:1–9.

Kawai, M., J. Wray, and K. Güth. 1990. Effect of ionic strength on crossbridge kinetics as studied by sinusoidal analysis, ATP hydrolysis rate, and X-ray diffraction techniques in chemically skinned rabbit psoas fibres. *J. Muscle Res. Cell Motil.* 11:392–402.

Krasner, B., and D. Maughan. 1984. The relationship between ATP hydrolysis and active force in compressed and swollen skinned muscle fibers of the rabbit. *Pfluegers Arch.* 400:160–165.

Levy, R. M., Y. Umazume, and M. J. Kushmerick. 1976. Ca^{2+} dependence of tension and ADP production in segments of chemically skinned muscle fibers. *Biochim. Biophys. Acta.* 430:352–365.

Lienhard, G. E., and I. I. Secemski. 1973. P^1,P^5-Di(adenosine-5′) pentaphosphate, a potent multisubstrate inhibitor of adenylate kinase. *J. Biol. Chem.* 248:1121–1123.

Matsubara, I., Y. Umazume, and N. Yagi. 1985. Lateral filamentary spacing in chemically skinned murine muscles during contraction. *J. Physiol.* 360:135–184.

Oosawa, F., S. Fujime, S. Ishiwata, and K. Mihashi. 1973. Dynamic property of F-actin and thin filament. *Cold Spring Harbor Symp. Quant. Biol.* 37:277–285.

Schoenberg, M. 1980. Geometrical factors influencing muscle force development. I. The effect of filament spacing upon axial forces. *Biophys. J.* 30:51–68.

Schoenberg, M. 1988. Characterization of the myosin adenosine triphosphate (M.ATP) crossbridge in rabbit and frog skeletal muscle fibers. *Biophys. J.* 54:135–148.

Shimizu, H., and H. Tanaka. 1984. Symmetric and asymmetric processes in the mechano-chemical conversion in the cross-bridge mechanism studied by isometric tension transients. *In* Contractile Mechanisms in Muscle. G. H. Pollack and H. Sugi, editors. Plenum Press, New York. 585–595.

Sleep, J. A., and R. L. Hutton. 1980. Exchange between inorganic phosphate and adenosine 5-triphosphate in the medium by actomyosin subfragment 1. *Biochemistry.* 19:1276–1283.

Takashi, R., and S. Putnam. 1979. A fluorimetric method for continuously assaying ATPase: application to small specimens of glycerol-extracted muscle fibers. *Analyt. Biochem.* 92:375–382.

Tawada, K., and M. Kawai. 1990. Covalent cross-linking of single muscle fibers from rabbit psoas increases oscillatory power. *Biophys. J.* 57:643–647.

Tregear, R. T., and J. M. Squire. 1973. Myosin content and filament structures in smooth muscle. *J. Mol. Biol.* 77:279–290.

Vianna, A. L. 1975. Interaction of calcium and magnesium in activating and inhibiting the nucleoside triphosphatase of sarcoplasmic reticulum vesicles. *Biochim. Biophys. Acta.* 410:389–406.

Winkelmann, D. A., T. S. Baker, and I. Rayment. 1991. Three-dimensional structure of myosin subfragment-1 from electron microscopy of sectioned crystals. *J. Cell Biol.* 114:701–713.

Zhao, Y., and M. Kawai. 1991. Low level compression of rabbit psoas fibers by dextran T-500 decreases the rate of reverse power stroke, and the high level compression decreases the rate of power stroke. *Biophys. J.* 59:375*a*. (Abstr).

Zhao, Y., M. Kawai, and J. S. Wray. 1993. The effect of the lattice spacing change on cross-bridge kinetics in rabbit psoas fibers. *In* Mechanism of Myofilament Sliding in Muscle Contraction. H. Sugi and G. H. Pollack, editors. Plenum Press, New York. In press.